NATIONAL ADVISORY COMMITTEE FOR AERONAUTICS

TECHNICAL NOTE 3418

THE ZERO-LIFT WAVE DRAG OF A PARTICULAR FAMILY OF UNSWEPT, TAPERED WINGS WITH LINEARLY VARYING THICKNESS RATIO

By Arthur Henderson, Jr., and Julia M. Goodwin

Langley Aeronautical Laboratory
Langley Field, Va.

Washington
May 1955

NATIONAL ADVISORY COMMITTEE FOR AERONAUTICS

TECHNICAL NOTE 3418

THE ZERO-LIFT WAVE DRAG OF A PARTICULAR FAMILY OF UNSWEPT, TAPERED WINGS WITH LINEARLY VARYING THICKNESS RATIO

By Arthur Henderson, Jr., and Julia M. Goodwin

SUMMARY

On the basis of linear theory, the zero-lift wave drag of a particular family of unswept, tapered wings with linearly varying thickness ratio and symmetrical parabolic-arc sections has been calculated. The case of the wing with a given root thickness ratio is given primary consideration in this paper with the view toward its use for missiles with all-movable fins where the root thickness must be large enough to allow for a rigid attachment to the trunnion and controlling mechanism. By comparing the drag for these wings with that for a corresponding constant-thickness-ratio wing with rhombic sections, it is found that the variable-thickness-ratio wings can be used to advantage with no serious structural penalties if the wings are assumed to have the same given root thickness ratio or the same internal volume.

INTRODUCTION

Zero-lift drag calculations have generally not been made for tapered wings with curved surfaces because the thickness functions, from which the source distributions are obtained, are usually of such a nature that the drag equations are nonintegrable, although in some cases pressure distributions may be found. References 1 and 2 present a numerical method for computing the pressure wave drag of delta and arrow plan-form wings; reference 1 is for biconvex, constant-thickness-ratio sections, and reference 2 determines the minimum wave drag for constant-thickness-ratio wings.

By modifying the equation which describes the surface of an unswept, tapered wing of biconvex section and constant thickness ratio, for which the drag has not yet been found analytically, an unswept, tapered wing of biconvex section and linearly varying thickness ratio is obtained for which the drag can be found. This is not a completely general wing in that the taper ratio is equal to the ratio of the tip thickness ratio to root thickness ratio. Nevertheless, it is of immediate practical interest,

particularly as applied to missiles with all-movable controls for which the primary consideration often is that the root thickness be large enough to allow for a rigid attachment of the wing to the trunnion and controlling mechanism without incurring any large stress concentrations. Since missile wings are often subjected to large, instantaneous deflections, the juncture of the wing and trunnion must be well designed.

The unswept wing was chosen for this investigation because, for the higher Mach numbers at which missiles and future aircraft will be operated, the unswept wing is generally superior to the swept wing as far as drag is concerned. As an illustration, figure 1, which is taken from figure 10(b) of reference 3, is presented. Figure 1 presents the ratio of the drag coefficient of a rectangular wing to the drag coefficient of an untapered, sweptback wing of the same aspect ratio (A = 5), plan-form area, thickness ratio, and parabolic-arc section as a function of Mach number for various angles of sweepback. After the leading edge of the sweptback wing becomes supersonic, the drag characteristics of the rectangular wing are seen to be as good as or superior to those of the sweptback wing. As the Mach number increases, the angle of sweepback necessary to reduce the drag below that of the rectangular wing becomes structurally unfeasible; therefore, the rectangular wing is preferable to the sweptback wing at the higher Mach numbers.

For a given thickness at the root, which is the primary concern in this paper, an unswept, tapered wing will have better drag characteristics than a rectangular wing of the same aspect ratio and plan-form area because the tapered wing will have a larger root chord and, consequently, a lower thickness ratio. A further decrease in the drag can be obtained by retaining the tapered plan form and the given root thickness ratio but reducing the local spanwise thickness ratio. Of course, this spanwise reduction in thickness ratio increases the local bending stresses so that, for any particular application, a satisfactory compromise between allowable stresses and drag reduction must be reached.

Since the higher Mach numbers are of interest and the wing of the present paper is unswept, the drag calculations have been made only for the case of supersonic leading edges.

SYMBOLS

A aspect ratio, $4s^2/S$

$B = \beta A$

C_D wave-drag coefficient, D/qS

C_{D_R} wave-drag coefficient of rectangular wing

C_{D_S} wave-drag coefficient of sweptback wing

$c(y)$ local chord

c_r root chord

D wave drag

F frontal area

$I_{xx}(y)$ moment of inertia about local chord

$K = \frac{2(1 - \lambda)}{1 + \lambda}$

M Mach number

$m(y)$ local bending moment

N sweepback parameter, $\frac{c_r(1 - \lambda)}{2s}$, tangent of leading-edge sweepback angle

Δp local pressure minus free-stream pressure

q dynamic pressure, $\frac{1}{2}\rho V^2$

$r = \frac{t_s/c_r}{\tau_r} \leq \frac{\lambda^2}{2}$

S plan-form area

S' area of integration

s semispan

$t(y)$ maximum local thickness of wing

t_r maximum root thickness

t_s skin thickness

V free-stream velocity

V_1 internal volume

w vertical perturbation velocity

x,y,z Cartesian coordinates

$\beta = \sqrt{M^2 - 1}$

Λ leading-edge sweepback angle

λ wing taper ratio, $\frac{\text{Tip chord}}{\text{Root chord}}$

ξ,η coordinates of source point

ρ free-stream density

$\sigma(y)$ maximum local bending stress, $\frac{m(y)\frac{t(y)}{2}}{I_{xx}(y)}$

$\tau(y)$ local thickness ratio, $\frac{t(y)}{c(y)}$

τ_r root thickness ratio, $\frac{t_r}{c_r}$

ϕ perturbation velocity potential

Unless otherwise denoted, primed symbols refer to the constant-thickness-ratio wing.

ANALYSIS

The surface of the variable-thickness-ratio wing of the present investigation has parabolic-arc sections as described by the equation

$$z = 2\tau_r c_r\left[\frac{x}{c_r} - \left(\frac{x}{c_r}\right)^2 - N\frac{y}{c_r} + N^2\left(\frac{y}{c_r}\right)^2\right] \tag{1}$$

The maximum-thickness line is at $x = c_r/2$. The projection of the maximum-thickness line on the yz-plane is described by

$$z = \frac{\tau_r c_r}{2}\left(1 - 2N\frac{y}{c_r}\right)^2$$

and the thickness ratio is

$$\frac{t(y)}{c(y)} = \tau(y) = \tau_r\left(1 - 2N\frac{y}{c_r}\right) \tag{2}$$

By using the definition of N, equation (2) may be rewritten as

$$\tau(y) = \tau_r\left[1 - (1 - \lambda)\frac{y}{s}\right] \tag{3}$$

from which

$$\frac{\tau(s)}{\tau_r} = \lambda \tag{4}$$

Thus, the wing which is treated herein is not completely general in that the ratio of the tip and root thickness ratios is directly related to the taper ratio. Nevertheless, equation (1) does allow the drag to be calculated for curved-surface airfoils of practical interest, as mentioned previously.

The linearized partial-differential equation for the perturbation potential in steady supersonic flow is

$$\beta^2\frac{\partial^2\phi}{\partial x^2} - \frac{\partial^2\phi}{\partial y^2} - \frac{\partial^2\phi}{\partial z^2} = 0 \tag{5}$$

If the disturbances are assumed to be small, the boundary conditions on the surface of a thin, symmetrical wing at zero angle of attack may be satisfied to the first order in the plane of the wing. Hence

$$\left(\frac{\partial\phi}{\partial z}\right)_{z=0} = w = \frac{dz}{dx}V \tag{6}$$

Reference 4 shows that a solution of equation (5) which satisfies condition (6) is, for a source distribution,

$$\phi(x,y)_{z=0} = -\frac{1}{\pi}\iint_{S'} \frac{w(\xi,\eta)\, d\xi\, d\eta}{\sqrt{(x-\xi)^2 - \beta^2(y-\eta)^2}} \tag{7}$$

where $w(\xi,\eta) = \frac{dz(\xi,\eta)}{d\xi}V$ is proportional to the source strength per unit area.

To the first order, the pressure in the plane of the wing is given by

$$\frac{\Delta p}{q} = -\frac{2}{V}\left(\frac{\partial \phi}{\partial x}\right)_{z=0} \tag{8}$$

The drag is expressed as

$$\frac{D}{q} = 2\iint_{S'} \frac{\Delta p}{q}\frac{dz}{dx}\, dx\, dy \tag{9}$$

and can be found by either of two essentially equivalent approaches.

The first method follows from reference 5 and is the more general of the two procedures. Since, for the zero-lift case, the potential in the $z = 0$ plane off the wing is zero, the potential at any point on the wing is the integrated effect on that point of all the sources within the wing boundaries which can influence that point. Thus, the wing of figure 2 has five regions of influence. The potential for each region can be found by integrating equation (7) over the area bounded by the wing plan form and the Mach lines which are drawn forward from the arbitrary point of each region. In practice, however, it is necessary to perform the integration only for the arbitrary point of region (5), since the potential for each of the other four regions consists of the appropriate real parts of the potential of region (5). The drag can therefore be found from equation (9) by integrating the product of the slope and the pressure for region (5) over the whole plan form and taking the appropriate real parts of the result.

The second method consists of the superposition of source distributions, a procedure which is described in reference 6. Although this method is not so straightforward as the first, its use is often advantageous, particularly if some previously calculated results are applicable, as was the case with the present paper. As shown in figure 3, there are

three regions over which equation (9) is applicable, subject in all three cases to the condition that $B > K$, that is $\beta A > \frac{2(1 - \lambda)}{1 + \lambda}$ (supersonic leading edges). These regions are:

$$\left.\begin{array}{l} \text{Region I: } B \geqq 2 \\ \text{Region II: } \frac{2\lambda}{1 + \lambda} \leqq B \leqq 2 \\ \text{Region III: } 0 \leqq B \leqq \frac{2\lambda}{1 + \lambda} \end{array}\right\} B > K$$

Thus, if a wing has a configuration with respect to the Mach lines that fits region II, the functions of equation (9) relating to regions I and II are real, and those for region III are imaginary.

The drag functions obtained from equation (9) have been evaluated by the second method and are given in the appendix for the three different regions. The drag is plotted in figure 4 as a function of $B = \beta A$ and λ.

RESULTS AND DISCUSSION

In addition to having good drag characteristics, a practical wing must be structurally sound. In order to ascertain the relative drag and structural properties of the present wing, the drag and maximum local bending stresses of the variable-thickness-ratio wing are compared with the same properties of a corresponding constant-thickness-ratio wing. The results for the constant-thickness-ratio wing which has rhombic sections are obtained from reference 7.

Given Root Thickness Ratio

Since the main application of the present wing is to missiles with all-movable fins where the thickness at the root must be sufficient for a rigid attachment of the wing to the trunnion and controlling mechanism, the drag and structural characteristics of a variable- and a constant-thickness-ratio wing of the same plan form should be made on the basis that they both have the same root thickness ratio. If primed symbols denote values pertaining to the constant-thickness-ratio wing (obtained from ref. 7) and unprimed symbols represent the variable-thickness-ratio wing, the ratio of the drags of the two wings on the basis of a given root thickness ratio is

$$\frac{C_D}{C_D'} = \frac{C_D\beta/\tau_r^2}{C_D'\beta/\tau_r'^2} \tag{10}$$

Equation (10) is presented in figure 5, from which C_D/C_D' is seen to be a strong function of λ, with drag reductions obtained for values of λ less than about 0.70.

It should be noted that the constant-thickness-ratio wing used for comparison has rhombic sections, which makes C_D/C_D' less favorable than if it had parabolic-arc sections (that is, for a given thickness ratio, a rhombic section has less wave drag than a parabolic-arc section). According to reference 8, if a constant-thickness-ratio wing has parabolic-arc sections, all values of C_D/C_D' should be multiplied by 0.75.

As indicated by linear theory, two identical plan forms at the same angle of attack will have the same lift distribution and, consequently, the same local bending moment. Since the maximum local bending stresses are

$$\sigma(y) = \frac{1}{2}\frac{m(y)t(y)}{I_{xx}(y)} \tag{11}$$

the ratio of the maximum local bending stresses of the solid variable-thickness-ratio wing to the constant-thickness-ratio wing is

$$\frac{\sigma(y)}{\sigma'(y)} = \frac{t(y)I_{xx}'(y)}{I_{xx}(y)t'(y)} \tag{12}$$

Now,

$$t(y) = \tau(y)c(y) \tag{13}$$

and

$$I_{xx} = 2\int_{L.E.(y)}^{T.E.(y)}\int_0^{z(x,y)} z^2 dz\, dx \tag{14}$$

Therefore,

$$\frac{\sigma(y)}{\sigma'(y)} = \frac{35\tau_r'^2}{64\tau_r^2\left[1 - (1 - \lambda)\frac{y}{s}\right]^2} \tag{15}$$

which, on the basis of given root thickness ratios, becomes

$$\left[\frac{\sigma(y)}{\sigma'(y)}\right]_{solid} = \frac{35}{64\left[1 - (1 - \lambda)\frac{y}{s}\right]^2} \tag{16}$$

Implicit in equation (15) is the assumption of solid wings. For large wings where, in order to reduce the weight, a hollow wing construction is used, calculation of I_{xx}, based on the assumption that the skin carries all the load, will probably more nearly represent the true state of affairs than does equation (15). For a wing with constant skin thickness t_s, where x_1 is the point on the x-axis where hollowness begins,

$$I_{xx} = 4\int_{L.E.(y)}^{x_1(y)}\int_0^{z(x,y)} z^2 dz\, dx + 4\int_{x_1(y)}^{c/2}\int_{z(x,y)-t_s}^{z(x,y)} z^2 dz\, dx \tag{17}$$

from which, by using equation (12),

$$\left[\frac{\sigma(y)}{\sigma'(y)}\right]_{hollow} = \frac{35r\tau_r'^2}{8\tau_r^2\left[1 - (1 - \lambda)\frac{y}{s}\right]^3} \times \frac{\left[1 - \frac{r}{1 - (1 - \lambda)\frac{y}{s}}\right]\left\{\left[1 - \frac{r}{1 - (1 - \lambda)\frac{y}{s}}\right]^2 + \frac{r^2}{\left[1 - (1 - \lambda)\frac{y}{s}\right]^2}\right\}}{1 - \left\{1 - \frac{2r}{\left[1 - (1 - \lambda)\frac{y}{s}\right]^2}\right\}^{7/2}} \tag{18}$$

where $r = \frac{t_s/c_r}{\tau_r} \leq \frac{\lambda^2}{2}$.

If the term to the 7/2 power is expanded and r is allowed to approach zero, then

$$\frac{\sigma(y)}{\sigma'(y)} = \frac{35\tau_r'^2}{56\tau_r^2\left[1 - (1 - \lambda)\frac{y}{s}\right]} \tag{19}$$

which, for given root thickness ratios, is

$$\left[\frac{\sigma(y)}{\sigma'(y)}\right]_{\text{hollow}} = \frac{35}{56\left[1 - (1 - \lambda)\frac{y}{s}\right]} \tag{20}$$

Equations (16) and (20) are plotted in figure 6, where the solid lines are for the solid wing and the dashed lines are for the hollow wing which has a skin thickness that approaches zero. The hatched portion between each set of solid and dashed lines represents varying degrees of skin thickness. From this figure it may be seen that a hollow variable-thickness-ratio wing generally compares more favorably with a hollow constant-thickness-ratio wing than the solid wings do.

A comparison of figures 5 and 6 reveals that, as the taper ratio is decreased below about 0.70, increasingly large drag reductions are obtained but with correspondingly large increases in the ratios of local bending stresses, especially in the vicinity of the tip. Within limits, however, this increase in outboard bending stresses is not serious. In figure 7 the ratio of local bending stresses to root bending stresses of a solid wing with a constant thickness ratio is plotted against the spanwise position, as an illustration. The curves are based on the conservative assumption of constant pressure distribution. It may be seen that, for all but the case of $\lambda = 0$, the outboard sections are highly understressed. That is, from a structural standpoint, in all but the case of $\lambda = 0$, a constant-thickness-ratio wing wastes material.

As a matter of interest, the drag and bending moment of the two wings can also be compared on the basis of given frontal area and given volume.

Given Frontal Area

The projected frontal area of a wing is

$$F = 2\int_0^s t(y)\,dy \tag{21}$$

from which

$$F = \frac{\tau_r c_r s}{6}\left(1 + \lambda + \lambda^2\right) \tag{22}$$

$$F' = \frac{\tau_r' c_r s}{4}(1 + \lambda) \tag{23}$$

For $F = F'$ with all plan-form dimensions the same,

$$\tau_r = \frac{3\tau_r'(1 + \lambda)}{2\left(1 + \lambda + \lambda^2\right)} \tag{24}$$

Substituting equation (24) into equations (10), (15), and (19), on the basis of a given frontal area, yields

$$\frac{C_D}{C_D'} = \frac{9(1 + \lambda)^2}{4(1 + \lambda + \lambda^2)^2} \frac{C_{D\beta}/\tau_r^2}{C_D'\beta/\tau_r'^2} \tag{25}$$

$$\left[\frac{\sigma(y)}{\sigma'(y)}\right]_{\text{solid}} = \frac{35(1 + \lambda + \lambda^2)^2}{144(1 + \lambda)^2\left[1 - (1 - \lambda)\frac{y}{s}\right]^2} \tag{26}$$

$$\left[\frac{\sigma(y)}{\sigma'(y)}\right]_{\text{hollow}} = \frac{35\left(1 + \lambda + \lambda^2\right)^2}{126(1 + \lambda)^2\left[1 - (1 - \lambda)\frac{y}{s}\right]} \tag{27}$$

Equations (25), (26), and (27) are plotted in figures 8 and 9 and show that, for all taper ratios, the drag of the variable-thickness-ratio wing is higher than the drag of the constant-thickness-ratio wing, whereas the stresses in the wing are lowered.

Given Volume

The internal volume of a wing is

$$V_i = 4\int_0^s \int_{L.E.(x)}^{T.E.(x)} z(x,y)\,dx\,dy \tag{28}$$

from which,

$$V_i = \frac{\tau_r c_r^2 s}{3}\left(1 + \lambda + \lambda^2 + \lambda^3\right) \tag{29}$$

$$V_i' = \frac{\tau_r' c_r^2 s}{3}\left(1 + \lambda + \lambda^2\right) \tag{30}$$

For $V_i = V_i'$ with all plan-form dimensions the same,

$$\tau_r = \frac{\tau_r'\left(1 + \lambda + \lambda^2\right)}{1 + \lambda + \lambda^2 + \lambda^3} \tag{31}$$

Substituting equation (31) into equations (10), (15), and (19), on the basis of a given internal volume, yields

$$\frac{C_D}{C_D'} = \frac{\left(1 + \lambda + \lambda^2\right)^2}{\left(1 + \lambda + \lambda^2 + \lambda^3\right)^2}\,\frac{C_D\beta/\tau_r^2}{C_D'\beta/\tau_r'^2} \tag{32}$$

$$\left[\frac{\sigma(y)}{\sigma'(y)}\right]_{solid} = \frac{35\left(1 + \lambda + \lambda^2 + \lambda^3\right)^2}{64\left(1 + \lambda + \lambda^2\right)^2\left[1 - (1 - \lambda)\frac{y}{s}\right]^2} \tag{33}$$

$$\left[\frac{\sigma(y)}{\sigma'(y)}\right]_{hollow} = \frac{35\left(1 + \lambda + \lambda^2 + \lambda^3\right)^2}{56\left(1 + \lambda + \lambda^2\right)^2\left[1 - (1 - \lambda)\frac{y}{s}\right]} \tag{34}$$

Equations (32), (33), and (34) are plotted in figures 10 and 11. These figures show that drag reductions are obtained for all taper ratios, whereas the structural characteristics are somewhat worsened by comparison with the constant-thickness-ratio wing. Reference to figure 7, however, shows that, within limits, these poorer structural characteristics are tolerable.

CONCLUDING REMARKS

On the basis of linear theory, the zero-lift wave drag of an unswept, tapered wing with linearly varying thickness ratio and parabolic-arc sections has been calculated. Although this wing is not completely general, in that the ratio of the tip thickness ratio to root thickness ratio is equal to the taper ratio, it is nevertheless of immediate practical interest for such applications as missiles with all-movable fins where the primary consideration is often that the thickness at the root be sufficient to allow a rigid attachment of the wing to the trunnion and control mechanism.

The drag and bending-stress characteristics have been compared with the corresponding characteristics of a constant-thickness-ratio wing of the same plan form but with rhombic sections on the basis of the same root thickness ratio, the same frontal area, and the same internal volume.

For the case of the same root thickness ratio, the primary concern of this paper, the ratio of the drag of the variable-thickness-ratio wing to the drag of the constant-thickness-ratio wing becomes less than 1.00 at a taper ratio of about 0.70. Decreasing the taper ratio decreases the drag ratio but increases the ratio of local bending stresses of the variable-thickness-ratio wing to the local bending stresses of the constant-thickness-ratio wing. This bending-stress ratio is a maximum at the tips. However, inasmuch as most constant-thickness-ratio wings, when designed for a given root bending moment, will be understressed outboard, an outboard increase in bending stress is not too serious, within limits.

Although the wings with the same frontal area were better structurally than those in the preceding case, the drag was adversely affected for all taper ratios.

For the wings with the same internal volume, the drag ratio is less than 1.00 for all taper ratios and, although the outboard stresses are increased slightly over those for the case of the same root thickness ratio, a limited increase in outboard bending stresses is not objectionable.

It appears, therefore, that for the cases of the same root thickness ratio and the same internal volume, a satisfactory compromise between drag and stress considerations can be reached which will allow the present wing to be used to advantage.

Langley Aeronautical Laboratory,
National Advisory Committee for Aeronautics,
Langley Field, Va., January 17, 1955.

APPENDIX

DRAG FUNCTIONS

The drag functions (eq.(9)) have been evaluated for the three regions indicated in figure 3 where $\beta A > \frac{2(1 - \lambda)}{1 + \lambda}$ or $B > K$. These functions are:

For $B \geqq 2$,

$$\left(\frac{C_{D\beta}}{\tau_r^2}\right)_I = \frac{128B}{\pi(1 + \lambda)^2\sqrt{B^2 - K^2}}\left\{\left[\frac{B^6 - 2B^4K^2 + 10B^2K^4 - 4K^6}{12K(B^2 - K^2)^3} + \frac{\lambda^4(B^2 - 2K^2)}{12K(B^2 - K^2)}\right]\cos^{-1}\frac{K}{B} + \frac{3B^4 - 28B^2K^2 + 10K^4}{36(B^2 - K^2)^{5/2}} - \frac{\pi\lambda^4(B^2 - 2K^2)}{12K(B^2 - K^2)} + \frac{\lambda^4}{12\sqrt{B^2 - K^2}}\right\} \tag{A1}$$

For $\frac{2\lambda}{1 + \lambda} \leqq B \leqq 2$,

$$\left(\frac{C_{D\beta}}{\tau_r^2}\right)_{II} = \left(\frac{C_{D\beta}}{\tau_r^2}\right)_I + \frac{128B}{\pi(1 + \lambda)^2\sqrt{B^2 - K^2}}\left\{\frac{\lambda^4(B^2 - 2K^2)}{12K(B^2 - K^2)}\cos^{-1}\frac{B^2(1 + \lambda) - 4(1 - \lambda)}{4B\lambda} - \frac{(1 - \lambda)^3\sqrt{B^2 - K^2}}{6K^2}\log_e\left|\frac{2 + \sqrt{4 - B^2}}{B}\right| + \left[\frac{B^2(7B^4 - 22B^2K^2 + 5K^4)}{12K(B^2 - K^2)^3} - \frac{2\lambda(2B^2 - K^2)}{3K(B^2 - K^2)} + \frac{\lambda^2(2B^2 - K^2)}{2K(B^2 - K^2)} - \frac{\lambda^3}{3K}\right]\cos^{-1}\frac{B^2(1 + \lambda) + 4(1 - \lambda)}{4B} + \left[\frac{-14B^4 + 67B^2K^2 - 23K^4}{36(B^2 - K^2)^{5/2}} + \frac{\lambda(28B^2 - 23K^2)}{36(B^2 - K^2)^{3/2}} - \frac{17\lambda^2}{36\sqrt{B^2 - K^2}} - \frac{\lambda^3}{12\sqrt{B^2 - K^2}}\right]\frac{(1 + \lambda)\sqrt{4 - B^2}}{4}\right\} \tag{A2}$$

For $0 \leqq B \leqq \frac{2\lambda}{1+\lambda}$,

$$\left(\frac{C_{D\beta}}{\tau_r^2}\right)_{III} = \left(\frac{C_{D\beta}}{\tau_r^2}\right)_{II} + \frac{128B}{\pi(1+\lambda)^2\sqrt{B^2-K^2}}\left\{\left[\frac{-8B^6+24B^4K^2-15B^2K^4+4K^6}{12K(B^2-K^2)^3} + \frac{2\lambda(2B^2-K^2)}{3K(B^2-K^2)} - \frac{\lambda^2(2B^2-K^2)}{2K(B^2-K^2)} + \frac{\lambda^3}{3K}\right]\cos^{-1}\frac{B^2(1+\lambda)^2+4\lambda(1-\lambda)}{2B(1+\lambda)} + \left[\frac{10B^4-37B^2K^2+12K^4}{36(B^2-K^2)^{5/2}} - \frac{\lambda(6B^4+40B^2K^2-36K^4)}{72K^2(B^2-K^2)^{3/2}} + \frac{\lambda^2(3B^2+5K^2)}{18K^2\sqrt{B^2-K^2}} - \frac{\lambda^3\sqrt{B^2-K^2}}{12K^2}\right]\frac{\sqrt{4\lambda^2-B^2(1+\lambda)^2}}{2} + \frac{(1-\lambda)^2\sqrt{B^2-K^2}}{12K^4}\left[2K^2(2+\lambda^2)-B^2(1-\lambda)^2\right]\log_e\left|\frac{2\lambda+\sqrt{4\lambda^2-B^2(1+\lambda)^2}}{B(1+\lambda)}\right|\right\} \quad (A3)$$

These equations are indeterminate for the case of $\lambda = 1$. In the limit as $\lambda \longrightarrow 1$, they reduce to

$$\left(\frac{C_{D\beta}}{\tau_r^2}\right)_I = \frac{16}{3} \quad (A4)$$

$$\left(\frac{C_{D\beta}}{\tau_r^2}\right)_{II} = \frac{16}{3} \quad (A5)$$

$$\left(\frac{C_{D\beta}}{\tau_r^2}\right)_{III} = \frac{32}{3\pi}\left[\sin^{-1}B - \frac{B\sqrt{1-B^2}}{4} + \frac{B(6-B^2)}{4}\log_e\left|\frac{1+\sqrt{1-B^2}}{B}\right|\right] \quad (A6)$$

REFERENCES

1. Beane, Beverly: The Characteristics of Supersonic Wings Having Biconvex Sections. Jour. Aero. Sci., vol. 18, no. 1, Jan. 1951, pp. 7-20.

2. Cooper, Morton, and Grant, Frederick C.: Minimum-Wave-Drag Airfoil Sections for Arrow Wings. NACA TN 3183, 1954.

3. Harmon, Sidney M.: Theoretical Supersonic Wave Drag of Untapered Sweptback and Rectangular Wings at Zero Lift. NACA TN 1449, 1947.

4. Puckett, Allen E.: Supersonic Wave Drag of Thin Airfoils. Jour. Aero. Sci., vol. 13, no. 9, Sept. 1946, pp. 475-484.

5. Evvard, John C.: Use of Source Distributions for Evaluating Theoretical Aerodynamics of Thin Finite Wings at Supersonic Speeds. NACA Rep. 951, 1950.

6. Henderson, Arthur, Jr.: Supersonic Wave Drag of Nonlifting Delta Wings With Linearly Varying Thickness Ratio. NACA TN 2858, 1952.

7. Nielsen, Jack N.: Effect of Aspect Ratio and Taper on the Pressure Drag at Supersonic Speeds of Unswept Wings at Zero Lift. NACA TN 1487, 1947.

8. Margolis, Kenneth: Some Remarks on an Approximate Method of Estimating the Wave Drag Due to Thickness at Supersonic Speeds of Three-Dimensional Wings With Arbitrary Profile. NACA TN 2619, 1952.

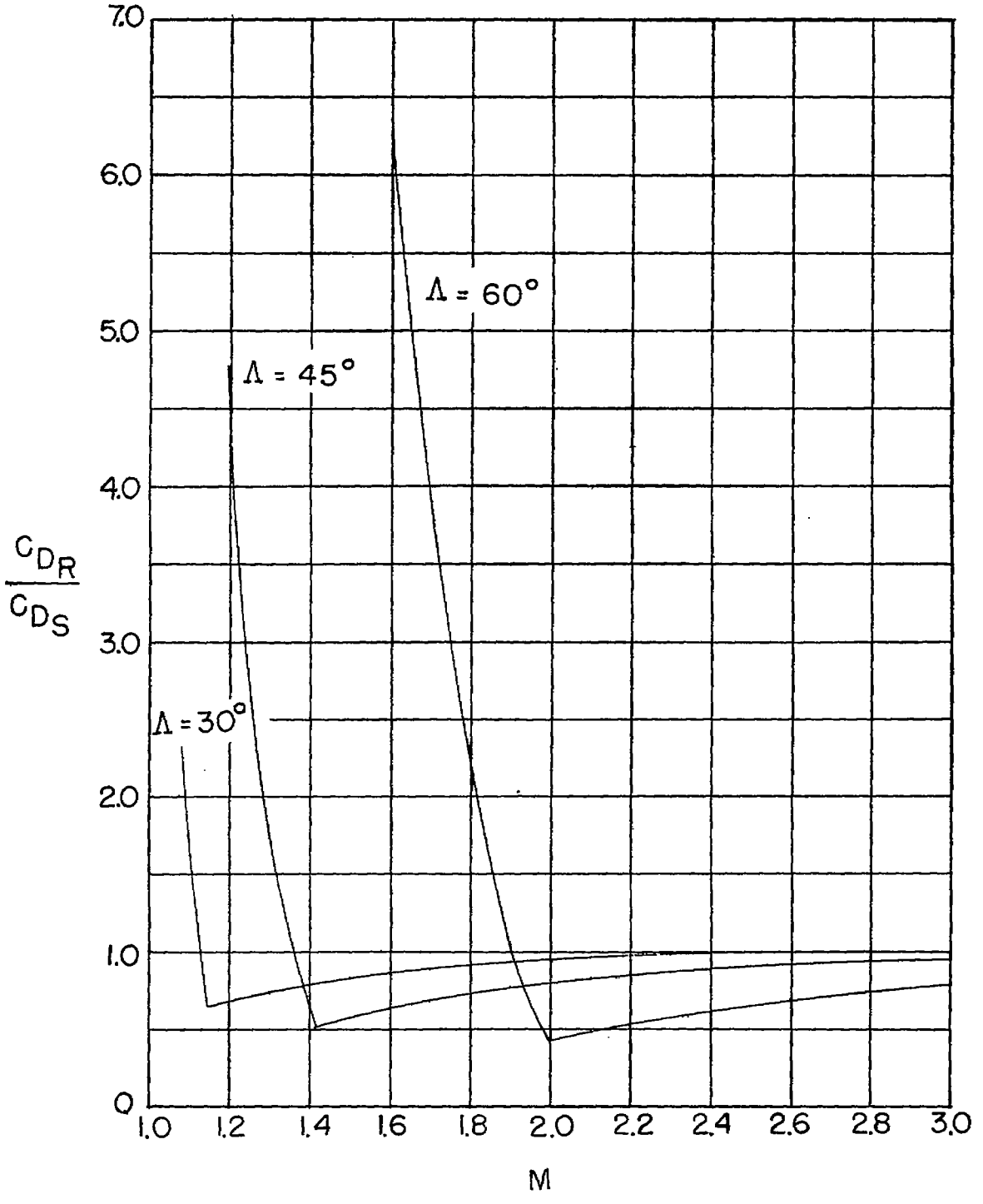

Figure 1.- Variation of ratios of wave-drag coefficient of rectangular wings to wave-drag coefficient of untapered, sweptback wings plotted against Mach number. Both wings have same plan form, parabolic-arc sections, and aspect ratio (A = 5).

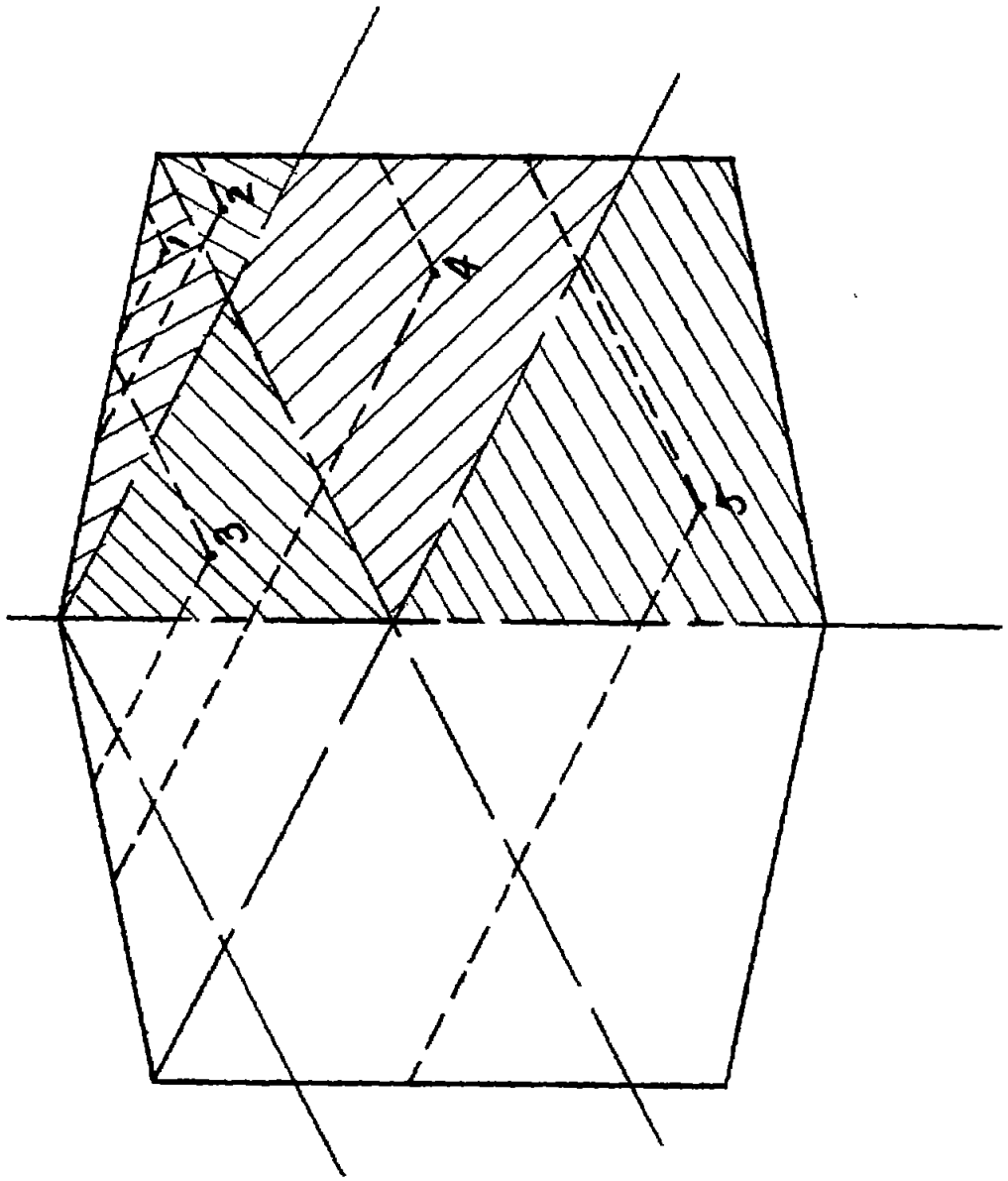

Figure 2.- Regions of influence for determining pressure distribution of an unswept, tapered wing.

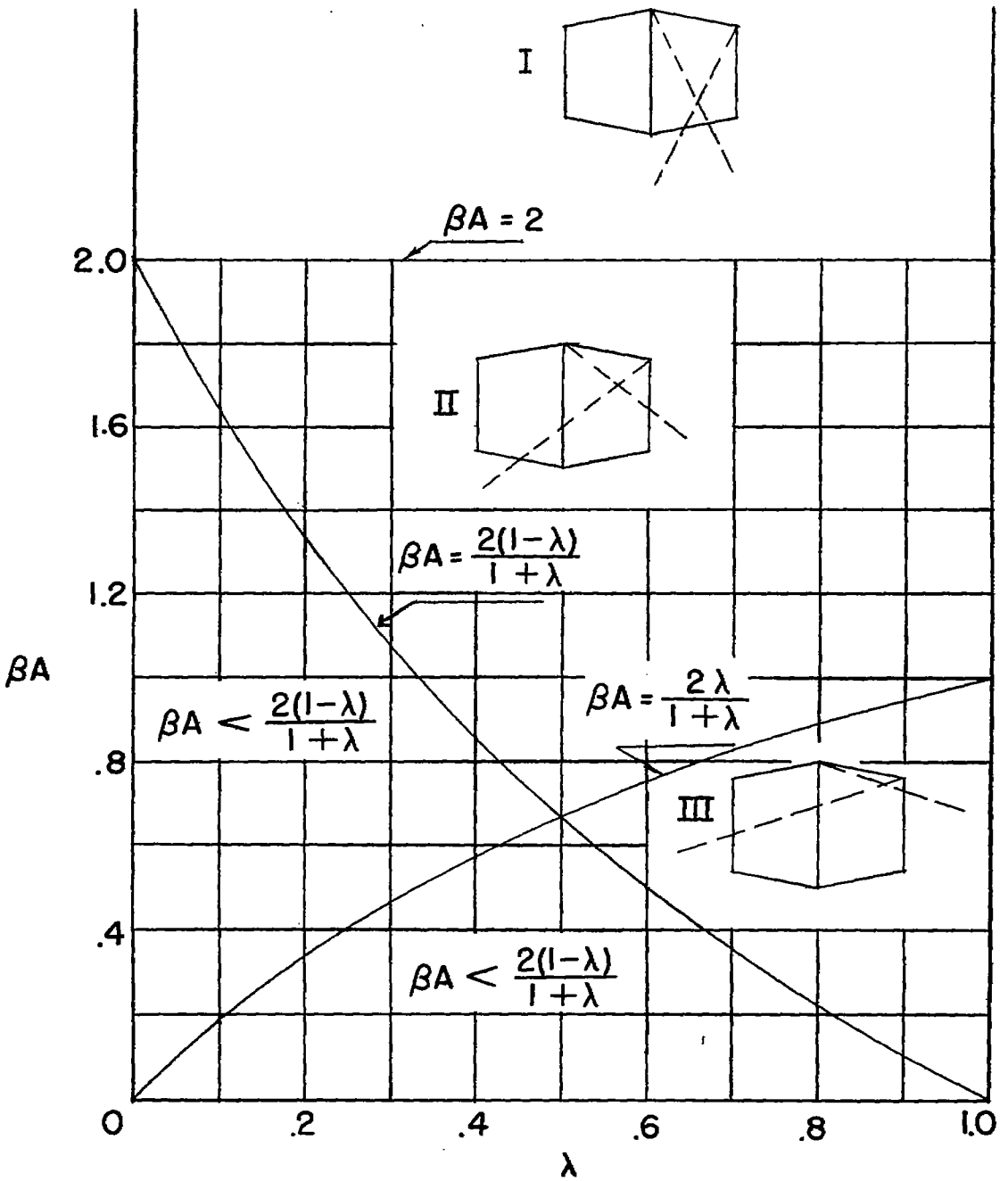

Figure 3.- Regions of applicability of equation (9).

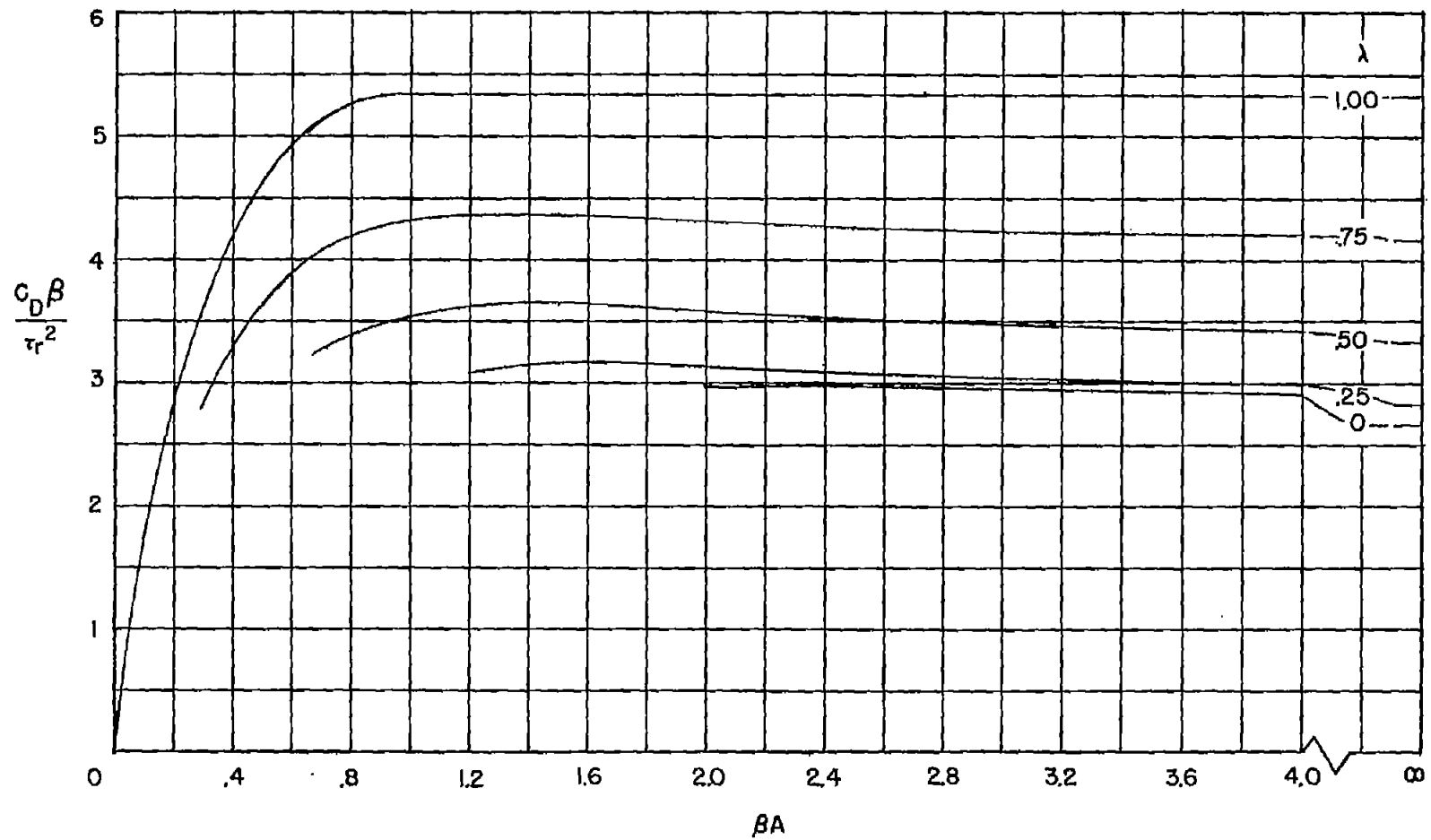

Figure 4.- Variation of zero-lift wave-drag coefficient of unswept wings having linearly varying thickness ratios and parabolic-arc sections with βA for various values of taper ratio.

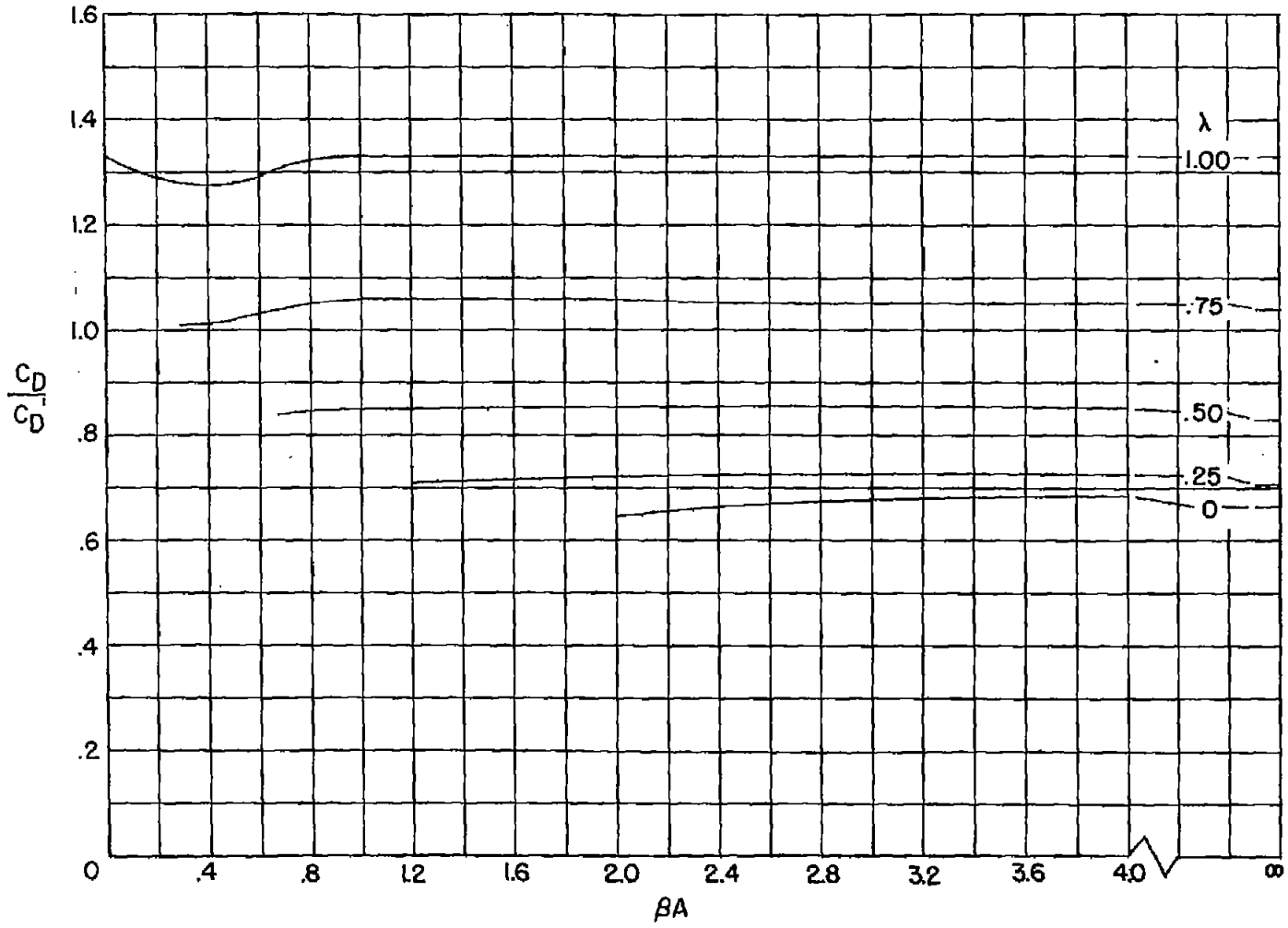

Figure 5.- Variation of ratios of wave-drag coefficients of variable-thickness-ratio wing and constant-thickness-ratio wing plotted against βA for various values of taper ratio.

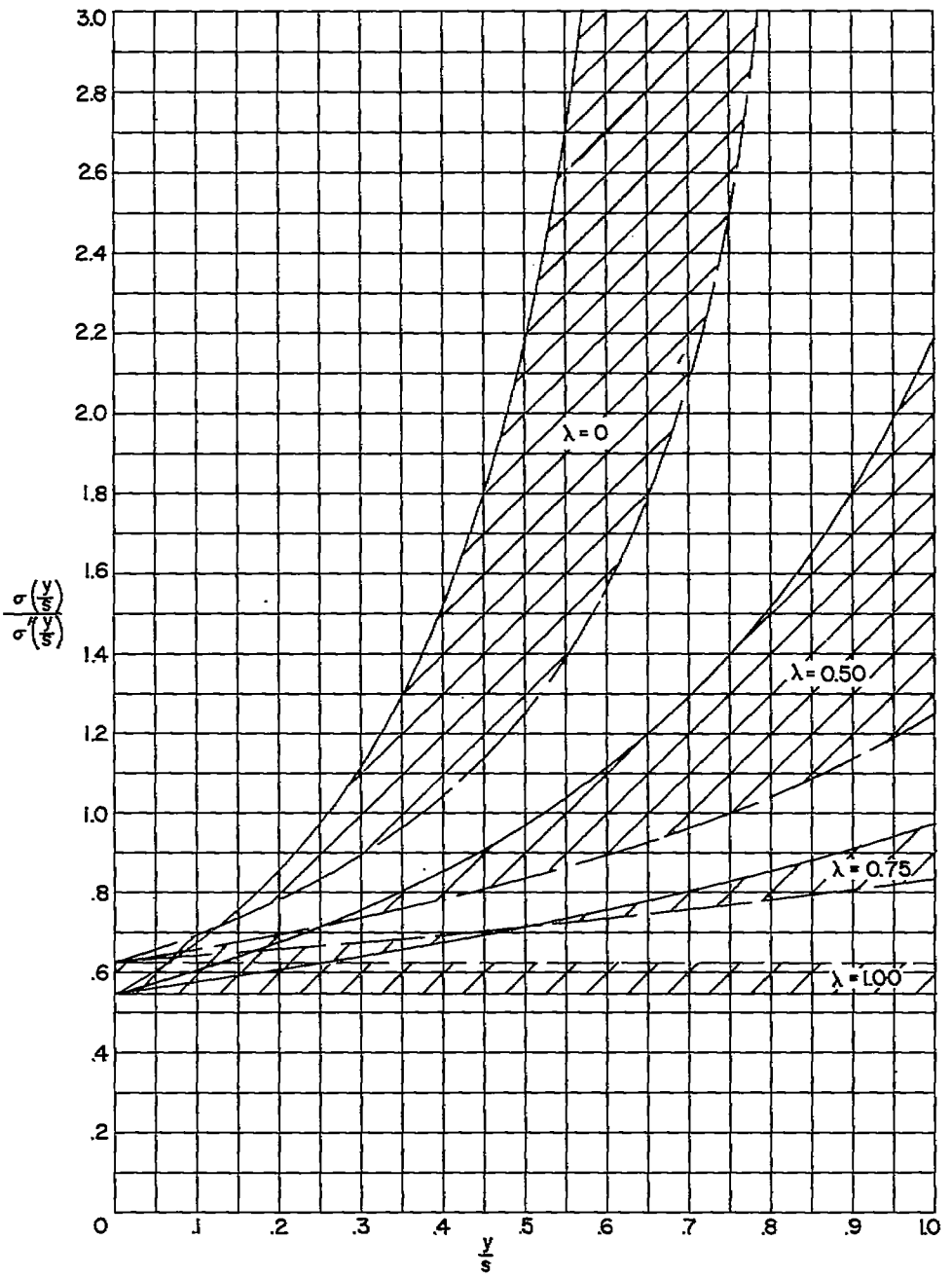

Figure 6.- Spanwise variation of ratio of $\frac{\sigma\left(\frac{y}{s}\right)}{\sigma'\left(\frac{y}{s}\right)}$ plotted against $\frac{y}{s}$ on basis of given root thickness ratio for various values of taper ratio. Solid lines indicate solid wing and dashed lines indicate wings which have a skin thickness which approaches zero.

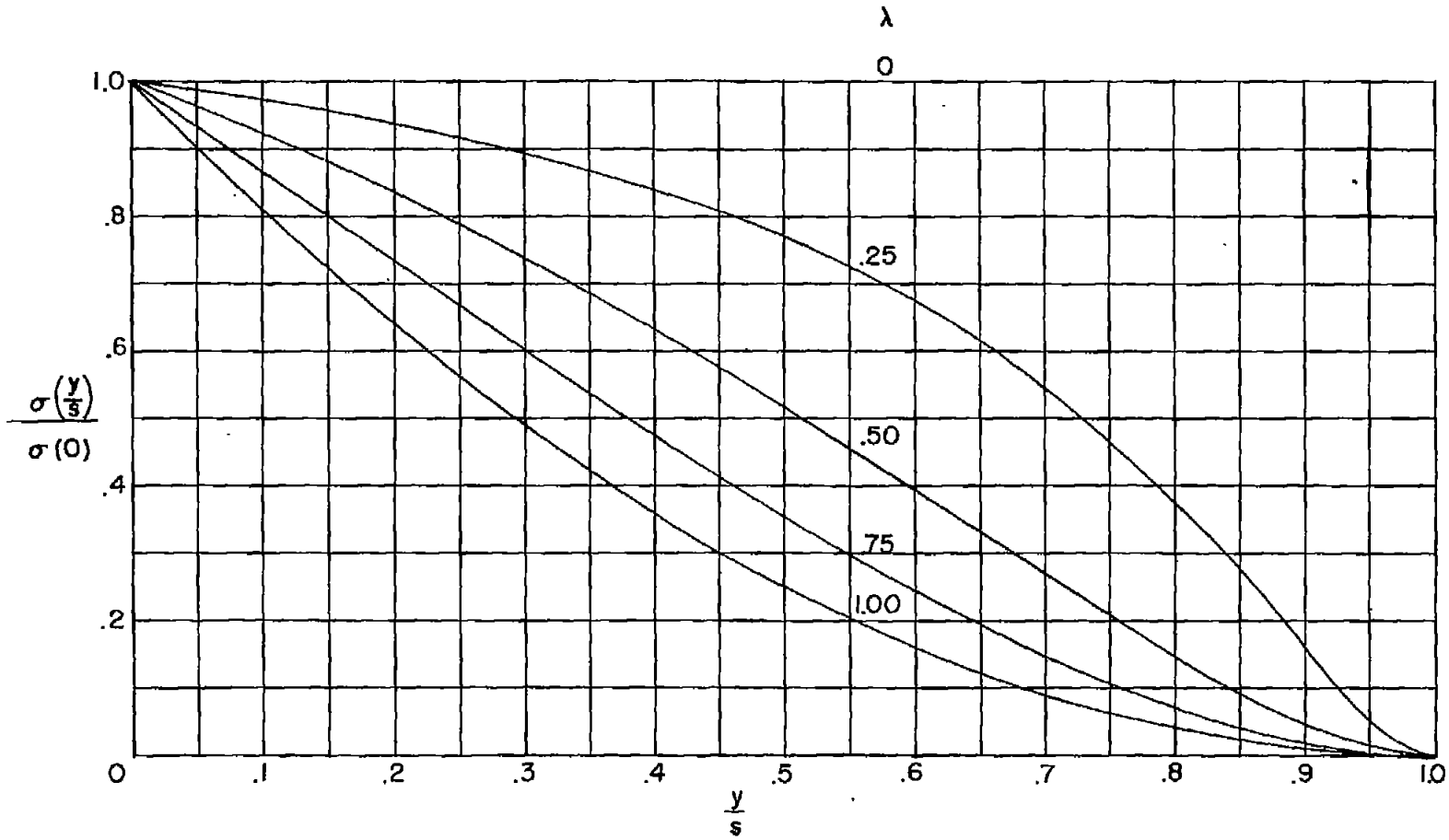

Figure 7.- Spanwise variation of ratio of $\frac{\sigma\left(\frac{y}{s}\right)}{\sigma(0)}$ plotted against $\frac{y}{s}$ for solid constant-thickness-ratio wing for various values of taper ratio.

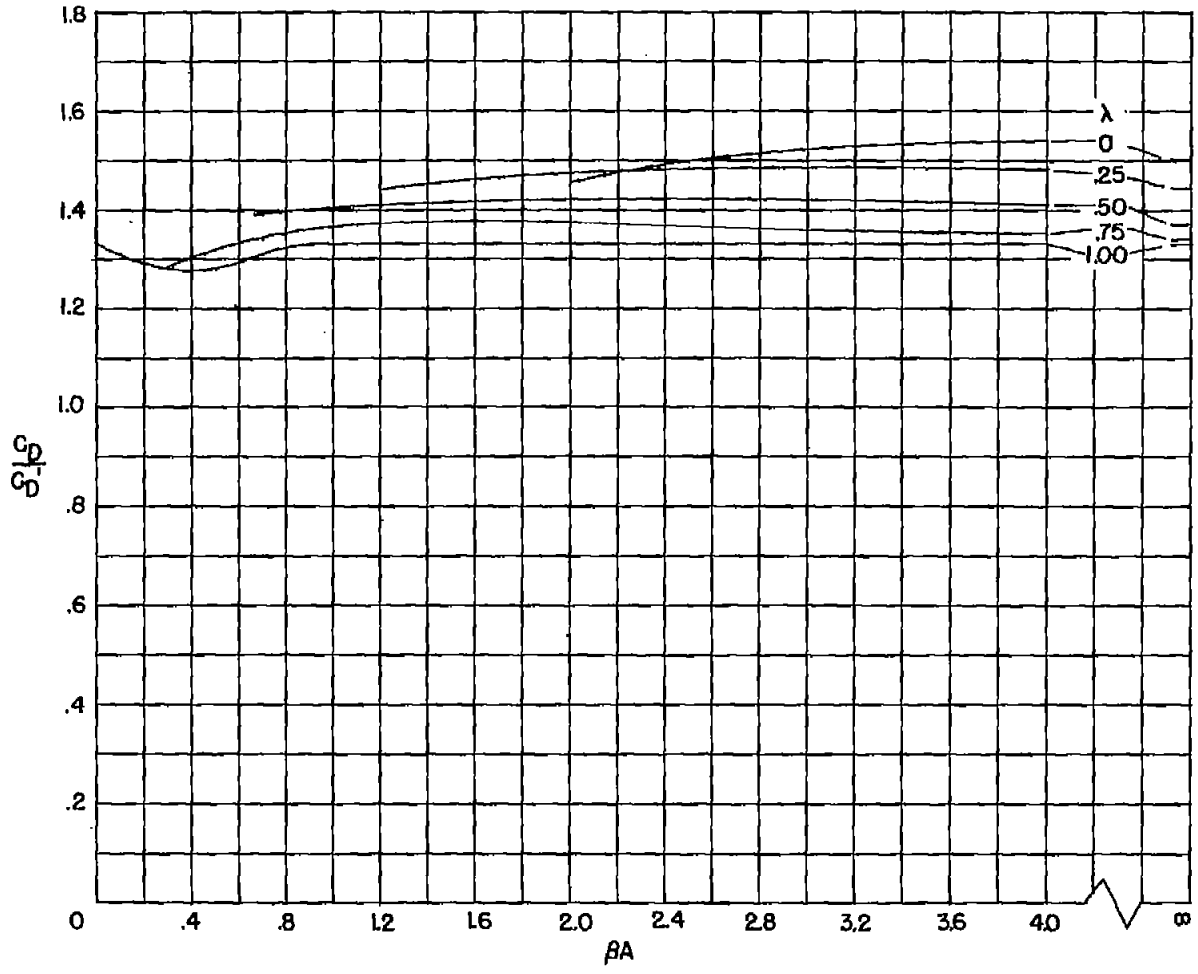

Figure 8.- Variation of ratios of wave-drag coefficients of variable-thickness-ratio wing and constant-thickness-ratio wing plotted against βA for various values of taper ratio. Both wings have same frontal area.

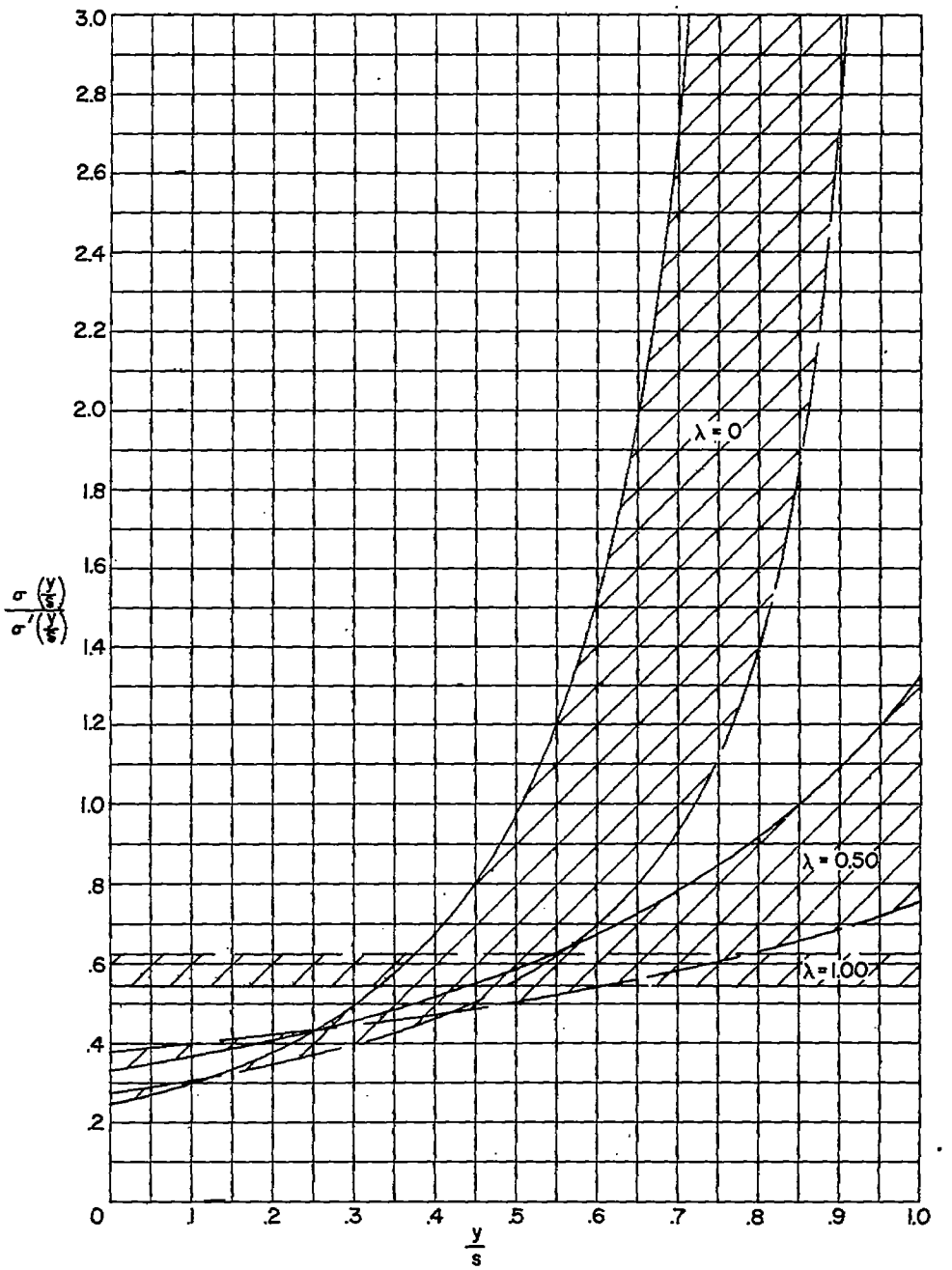

Figure 9.- Spanwise variation of ratio of $\frac{\sigma\left(\frac{y}{s}\right)}{\sigma'\left(\frac{y}{s}\right)}$ plotted against $\frac{y}{s}$ on basis of same frontal area for various values of taper ratio. Solid lines indicate solid wing and dashed lines indicate wings which have a skin thickness which approaches zero.

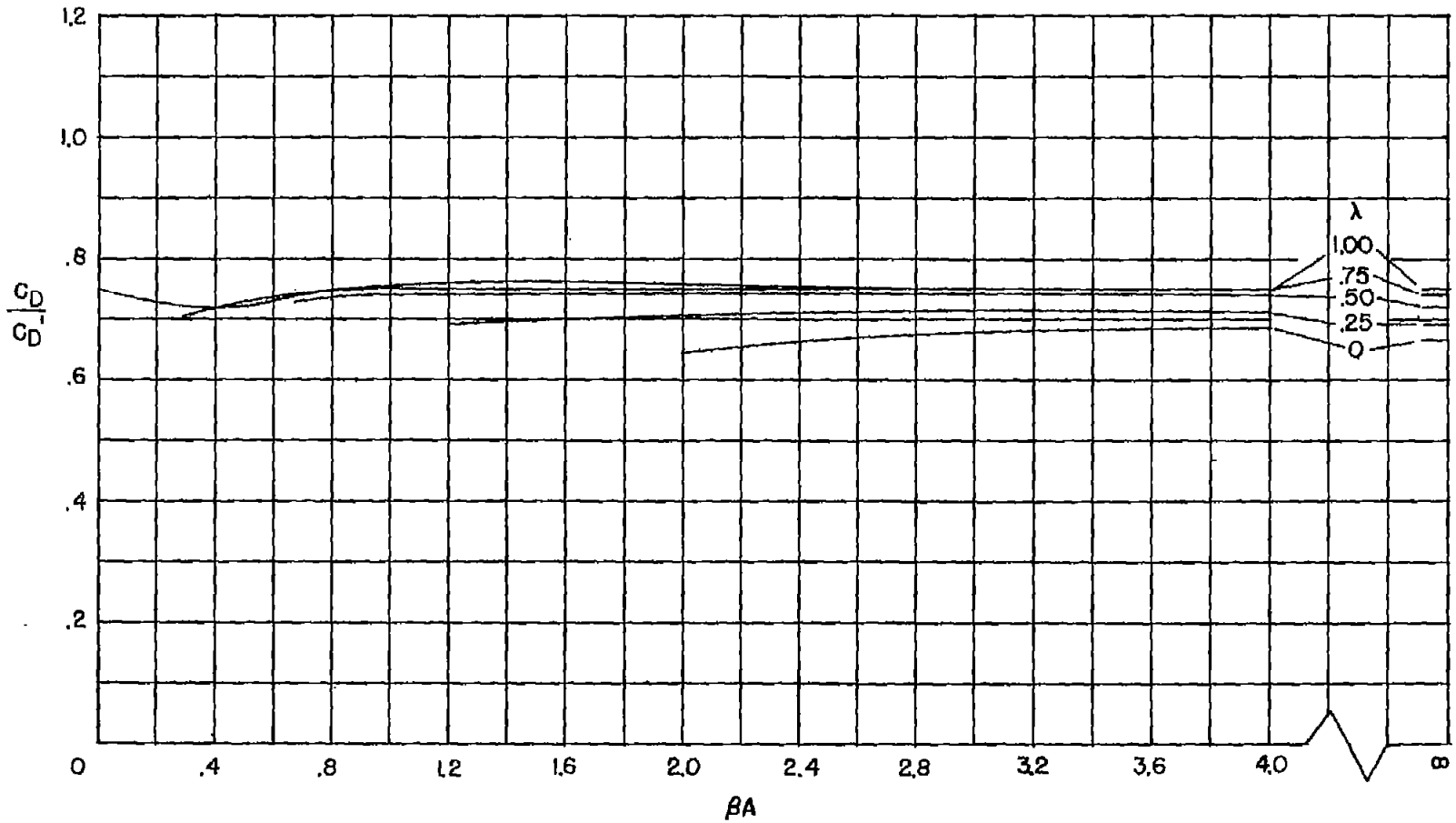

Figure 10.- Variation of ratio of wave-drag coefficients of variable-thickness-ratio wing and constant-thickness-ratio wing plotted against βA for various values of taper ratio. Both wings have same internal volume.

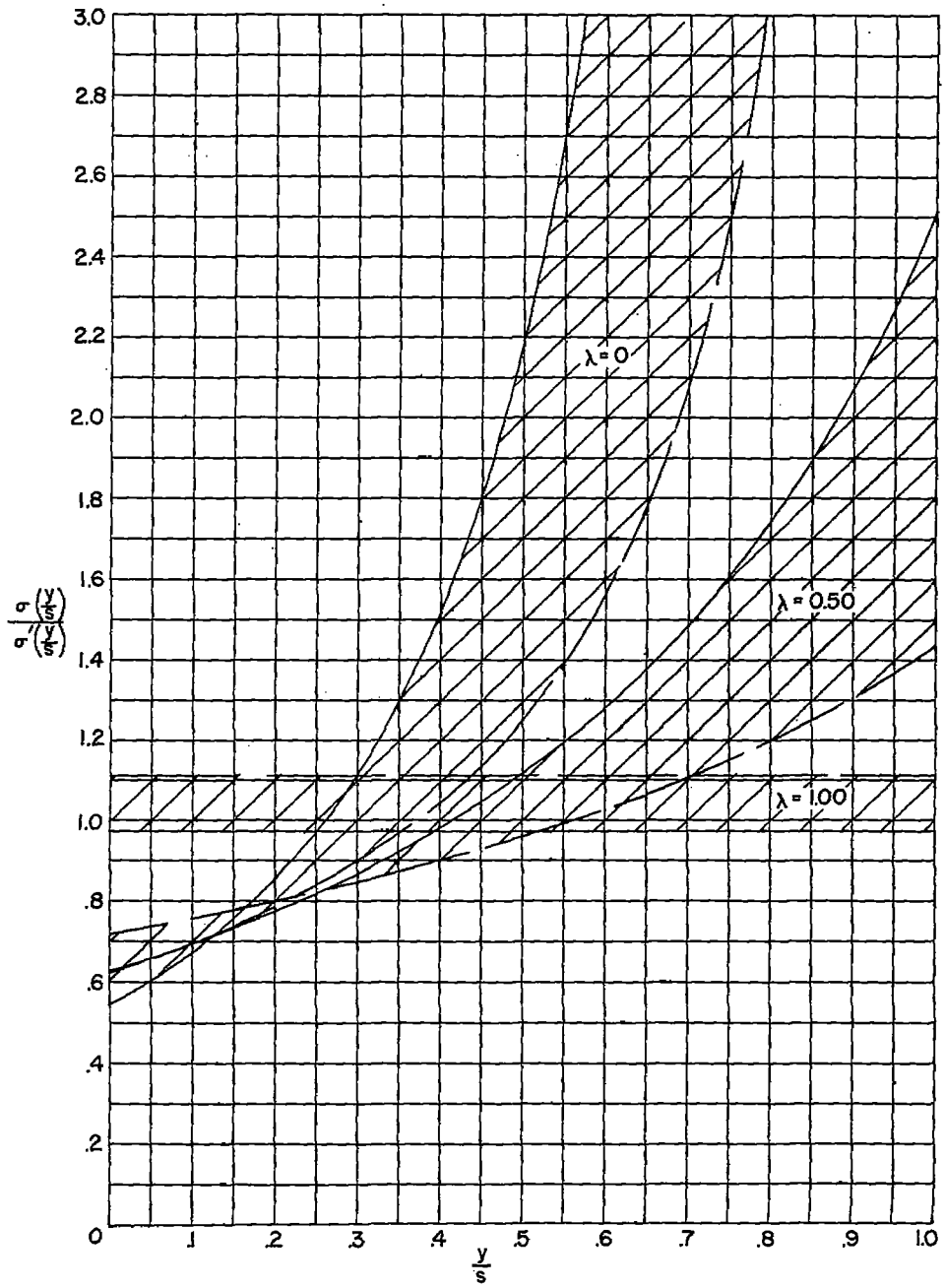

Figure 11.- Spanwise variation of ratio of $\frac{\sigma\left(\frac{y}{s}\right)}{\sigma'\left(\frac{y}{s}\right)}$ plotted against $\frac{y}{s}$ on basis of same internal volume for various values of taper ratio. Solid lines indicate solid wing and dashed lines indicate wings which have a skin thickness which approaches zero.

NACA-Langley - 5-4-55 - 1000